Green synthesis of *Quercus coccifera* hydrochar in subcritical water medium and evaluation of its adsorption performance for BR18 dye

Mohammed Saleh, Zeynep Bilici, Yasin Ozay, Erdal Yabalak, Mutlu Yalvac and Nadir Dizge

ABSTRACT

In this study, we investigated the production conditions of *Quercus coccifera* hydrochar, which is an inexpensive and easy available adsorbent, for the adsorption of Basic Red 18 (BR18) azo dye. The hydrochar was produced in the eco-friendly subcritical water medium (SWM). The effects of the pH (2–10), adsorbent size (45–106 μm), adsorbent dose (0.5–1.5 g/L), dye concentration (40–455 mg/L), and contact time (5–120 min) were studied via optimization experiments. The optimum conditions were pH 10, particle size of 45 μm, particle amount of 1.5 g/L, dye concentration of 455 mg/L, and 60 min. The removal efficiency increased sharply for the first 5 min; after that the removal efficiency reached a steady state at 60 min, with a maximum removal of 88.7%. The kinetic studies for the adsorption of BR18 dye in aqueous solution using hydrochar showed pseudo-second-order kinetics. The Langmuir and Freundlich isotherm models were used to explain the relationship between adsorbent and adsorbate, and Freundlich isotherm was the most suitable model because of its high regression coefficient (R^2) value. The intraparticle diffusion model was used to determine the adsorption mechanism of BR18 onto *Q. coccifera* acorn hydrochar. Desorption studies were also carried out using different types of acid and different molarities.

Key words | azo dye adsorption, hydrochar, *Quercus coccifera*, subcritical water

Mohammed Saleh
Zeynep Bilici
Yasin Ozay
Mutlu Yalvac
Nadir Dizge
Department of Environmental Engineering,
Mersin University,
33343 Mersin,
Turkey

Erdal Yabalak (corresponding author)
Department of Chemistry,
Mersin University,
33343 Mersin,
Turkey
and
Department of Nanotechnology and Advanced Materials,
Mersin University,
33343 Mersin,
Turkey
E-mail: *yabalakerdal@gmail.com*

HIGHLIGHTS

- Hydrochar from *Q. coccifera* was produced using subcritical water to obtain a solid product.
- The hydrochar was used as adsorbent to remove BR18 dye from aqueous solution.
- Hydrochar showed the highest dye removal efficiency of 88.7%, with 194.6 mg/g adsorption capacity.
- The equilibrium adsorption was best described by the Freundlich isotherm.

doi: 10.2166/wst.2020.607

GRAPHICAL ABSTRACT

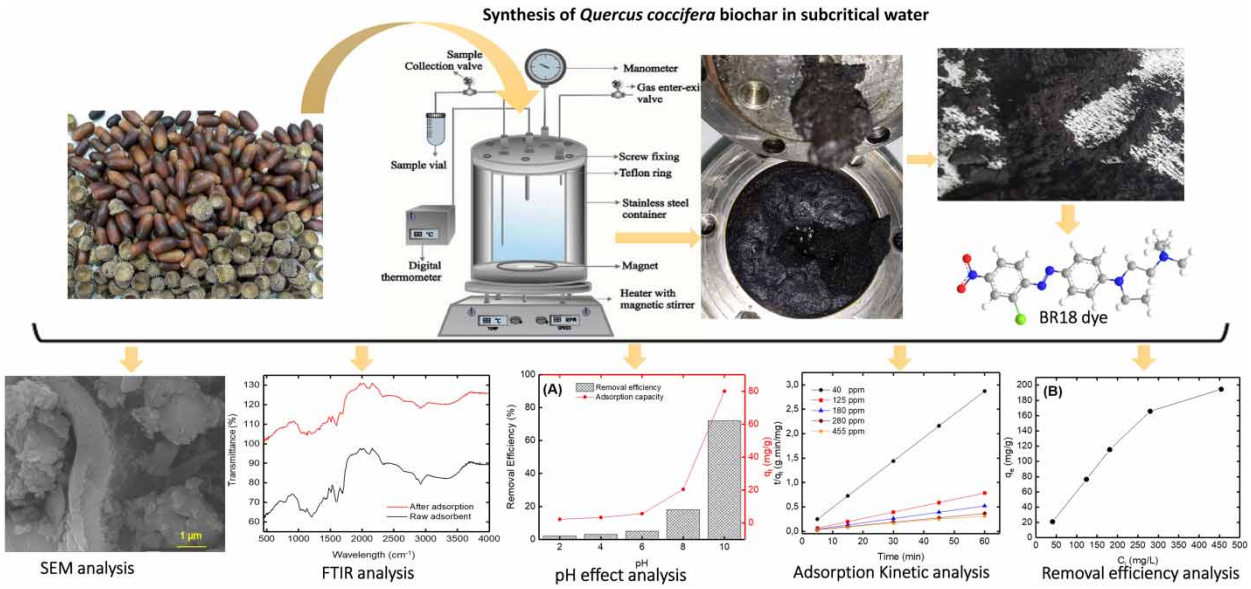

INTRODUCTION

Water pollution is a global issue (Saleh *et al.* 2019), and the textile industry is a major source of pollutants as it generates hazardous and colored wastewater that has harmful effects on human life and the environment (Patel & Vashi 2015). Textile wastewater is 3 billion tons over the world (Antczak *et al.* 2019; Li & Wang 2019). Cationic dyes like Basic Red 18 (BR18) reduce the transparency of water and therefore prevent sunlight from traveling through the water column, which in turn negatively affects the flora and fauna present (Nagpal & Kakkar 2020). Chong *et al.* (2014) stated that cationic dyes are carcinogenic and do not degrade naturally.

So far, many researchers have tried to treat dyes in wastewater using different methods. For the biological treatment systems, bacteria (Pearce *et al.* 2006; Lavanya *et al.* 2014), algae (Elumalai & Saravanan 2016), fungi (Krastanov *et al.* 2013), enzymes (Darwesh *et al.* 2019), and yeast (Martorell *et al.* 2018) have been used in the biodegradation of dyes. Chemical treatment methods have also been used: advanced oxidation processes (AOPs) (Al-Kdasi *et al.* 2004; Miklos *et al.* 2018), coagulation-flocculation (Verma *et al.* 2012; Dotto *et al.* 2019), electrocoagulation (EC) (Naje *et al.* 2016), electro-Fenton (EF) (Rosales *et al.* 2009), and anodic oxidation (AO) (dos Santos *et al.* 2019). Except for electrochemical methods, chemical treatment is more expensive than biological methods (Crini & Lichtfouse 2019). The mass transfer concept has also been used to remove dyes from wastewater using physical processes. They include the adsorption (Rafatullah *et al.* 2010), membrane filtration (Jegatheesan *et al.* 2016), and ion-exchange methods (Bayramoglu *et al.* 2020). The low cost, simplicity of design, high efficiency, and easy operation make the adsorption process more favorable than others (Asfaram *et al.* 2017).

The principle of the adsorption process is the attachment of the adsorbate onto the surface of the solid adsorbent. Based on the manner of attachment, the adsorption process can be categorized into physisorption or chemisorption (Gupta & Suhas 2009). Different materials have been used as adsorbents for dye removal: activated carbon (Tan *et al.* 2008), alumina (Banerjee *et al.* 2019), zeolite (Brião *et al.* 2018), bio-adsorbents (Gupta *et al.* 2014), biochar (Biswas *et al.* 2020), and subcritical water hydrolysis (Abaide *et al.* 2019).

Biochar is a stable carbon-rich solid obtained by different methods from different types of biomass. Subcritical water medium (SWM) has been used as an effective medium in synthesis, extraction, oxidation, solubility processes, and many other fields. It also provides a unique

medium for converting carbonaceous materials into hydrochar (Nural *et al.* 2018; Yabalak 2018a; Lee *et al.* 2019). Subcritical water is defined as water heated in range of 373–647 K and pressurized enough to keep the water liquid at this temperature (Yabalak 2018b). Conversion of biomass to hydrochar in SWM is an advantageous alternative to classical torrefaction, pyrolysis, or gasification because it provides a high conversion yield of biomass to hydrochar and water-soluble components of the biomass that cannot be obtained by other methods (Chuntanapum & Matsumura 2009; Kumar & Gupta 2009). In addition, subcritical water provides a reactive medium based on its molecular properties and SWM is more economical since it does not require a pre-drying step, with its attendant high costs (Chuntanapum & Matsumura 2009). Recently, the production of biochar, especially hydrochar, and their usage in various processes in environmental and agricultural applications have received great attention. Furthermore, it has been reported that biochar is highly effective for removing many organic pollutants from water and soil (Fang *et al.* 2014). To the best of our knowledge, this is the first attempt to investigate the production of hydrochar from *Quercus coccifera* L. in unique eco-friendly SWM as well as evaluating its effects as an adsorbent for the removal of dye contaminant in aqueous solution.

MATERIALS AND METHODS

Collection and preparation of *Q. coccifera* L.

Q. coccifera acorns were collected on 21 October 2018 from an open field in Akkent (Yenişehir, Mersin), which is 20–40 m above sea level. The complete fruit (nut and cup) was washed with distilled water to remove the resin and other impurities and kept at room temperature in the dark for 20 days until completely dry.

Hydrochar production in the subcritical water medium

A home-made stainless-steel reactor, which was described in detail in previous work, was used for the production of hydrochar in the SWM (Yabalak 2018b). The production process is schematized in Figure 1. Briefly, 30 g of dried *Q. coccifera* acorns were put into the reactor along with 150 mL of pure water. After closing the reactor, the inner pressure was raised to 100 bar. The temperature of the reactor was increased to 513 K and kept constant for 3 hours. At the end of the treatment time, the reactor was depressurized and opened. The obtained hydrochar was filtered through ordinary filter paper and dried in an oven at 373 K. 21.8 g of dry hydrochar was obtained, meaning a 72.8% hydrochar yield from the *Q. coccifera*. This value is quite high compared to pyrolysis, dry torrefaction, gasification, and even hydrothermal carbonization methods reported in literature (Lee *et al.* 2019).

Adsorbate preparation

In this study, a cationic dye (Basic Red 18; BR18) was examined. The properties of BR18 dye are shown in Table 1. A stock solution (1,000 ppm) was prepared and kept until the end of the experiments. The proposed concentrations were diluted from the stock solution. Sodium hydroxide (NaOH) and sulfuric acid (H_2SO_4) with different molarities (1–5) M were used to adjust the pH.

Figure 1 | The hydrochar production process in the SWM.

Table 1 | Properties of cationic BR18 dye (Fathy *et al.* 2017)

Chemical formula	$C_{19}H_{25}ClN_5O_2$
Chemical structure (2D)	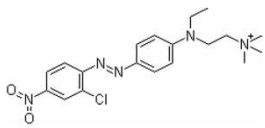
Chemical structure (3D)	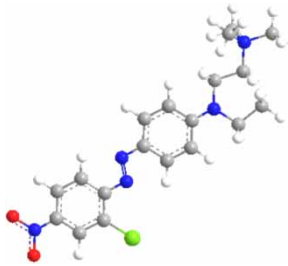
Molecular weight (g/mol)	390.89
Wavelength (nm)	486

Adsorbent characterization

Brunauer-Emmett-Teller (BET) analysis was employed to determine the surface area, total pore volume, microporous volume, and pore diameter using adsorption and desorption isotherms of N_2 gas (MicroActive for TriStar II Plus 2.00). The adsorbent surface area was determined by plotting the linear form of the BET equation. The total volume was calculated at the relative pressure (p/p_0) 0.99 (Schneider 1995). The microporous volume and the pore diameter were determined by the method of Boer and by the ratio of 4 V_{total}/BET surface, respectively (Barrett *et al.* 1951).

The adsorbent surface morphology was observed by scanning electron microscope (SEM; Zeiss, Supra 55).

Fourier transform infrared spectroscopy (FT/IR-6700, Jasco) was utilized to investigate the functional groups present on the surface of the adsorbent. The functional groups were scanned for bands between 450 and 4,000 cm^{-1}.

The surface charge changes of the prepared hydrochar during the pH optimization were measured using zeta potential (Malvern Zeta Sizer Nano ZS).

Batch studies

The adsorption of the cationic dye (BR18) onto the prepared hydrochar was assessed by the batch method. All the experiments were carried on 50 mL solutions using 250 mL Erlenmeyer flasks (Isolab). They were agitated at a speed of 155 rpm using an orbital shaker (Biosan PSU-20i) at room temperature ($25 \pm 2\,^{\circ}C$). The changes in dye concentration were measured using a spectrophotometer (Hack DR-3900) at the previously stated wavelengths. The removal efficiencies and adsorption capacities were calculated using Equations (1) and (2), respectively:

$$\text{Removal efficiency (\%)} = \frac{(C_i - C_e)}{C_i} \times 100 \quad (1)$$

$$q_e = \frac{(C_i - C_e) \times V}{m} \quad (2)$$

where C_i and C_e are the concentration of the dye before and after the adsorption process (mg/L), q_e is the adsorption capacity (mg/g), V is the volume of the aqueous solution (L), and m is the mass of the prepared hydrochar (g).

The effects of pH (2–10), adsorbent size (45–150 μm), adsorbent dose (0.5–1.5 g/L), dye concentration (50–455 mg/L), and contact time (5–120 min) were studied via optimization experiments. The optimum conditions were obtained by studying the factors one by one.

Adsorption kinetics

In this study, Lagergren's pseudo-first-order model (Equation (3)) and pseudo-second-order model (Equation (4)) were used to describe the adsorption of BR18 onto the prepared adsorbent. The samples were collected over time until the final concentrations were very close to each other. The obtained data were linearized, and the correlation coefficients were calculated.

$$\text{Log}\ (q_e - q_t) = \log q_e - \frac{K_1}{2.303} t \quad (3)$$

$$\frac{t}{q_t} = \frac{1}{K_2 q_e^2} + \frac{1}{q_e} t \quad (4)$$

where q_e and q_t are the adsorption capacities at equilibrium and time t (mg/g), K_1 is Lagergren's constant (1/min), K_2 is the second-order constant (mg/g·min).

The Weber–Morris equation or intraparticle diffusion assumes that intraparticle diffusion is the rate-limiting step in the overall biosorption process, as shown in Equation (5):

$$q_t = k_i t^{0.5} + C \quad (5)$$

where k_i is the intraparticle diffusion rate constant (mg·g·$min^{-1/2}$), C is a boundary layer thickness constant.

Table 2 | The linear forms of the examined isotherms

Isotherm	Linear form	Plot	Equation
Langmuir	$C_{BR}/q_{BR} = 1/(b_{BR}q_m) + C_{BR}/q_m$	C_{BR} versus $C_{BR}\backslash q_{BR}$	(6)
Freundlich	$Log(q_{BR}) = \log(K_{BR}) + (1/n)\log(C_{BR})$	$LogC_{BR}$ versus $Logq_{BR}$	(7)
Tempkin	$q_{BR} = RT/b_T LnA_T + RT/b_T lnC_{BR}$	LnC_{BR} versus q_{BR}	(8)
Dubinin-Radushkevich (D-R)	$Lnq_{BR} = Lnq_s - K_{ad}[RTLn(1 + 1/C_{BR})]^2$	$[RTLn(1 + 1/C_{BR})]^2$ versus Ln q_{BR}	(9)
Redlich-Peterson (R-P)	$\ln\left(\frac{C_{BR}}{q_{BR}}\right) = \beta \ln C_{BR} + Lna_r$	LnC_{BR} versus $Ln(K_rC_{BR}/q_{BR} - 1)$	(10)
Sips	$\frac{1}{q_{BR}} = \frac{1}{q_m K_s}\left(\frac{1}{C_e}\right)^{1/r} + \frac{1}{q_m}$	$(1/C_e)^{1/r}$ versus $1/q_{BR}$	(11)

where C_{BR} is the equilibrium concentration of the BR18 (mg/L), b_{BR} is the Langmuir constant for BR18 (L/mg), q_m is the maximum adsorbent capacity at saturation (mg/g), K_{BR} is the Freundlich adsorption capacity parameter (mg/g).(L/mg), 1/n is the intensity parameter, R is the universal gas constant (8.314 J/K·mol), T is the absolute temperature (K), b_T is the Tempkin isotherm constant, A_T is the binding constant (L/g), q_s is the theoretical saturation capacity (mg/g), K_{ad} is the isotherm constant (mol^2/kJ^2), β is the exponent lies between 0 and 1, a_r is R-P isotherm constant (L/g), K_S is the Sips constant (1/mg).

Adsorption isotherm

The adsorption isotherm is important for clarifying the interaction between the adsorbent and the adsorbate. Isotherm experiments were carried out by changing the adsorbent dose while the other factors were kept unchanged. The initial concentration, final concentration, the adsorption capacities were plotted using the linear form of the Langmuir (Langmuir 1918), Freundlich (Freundlich 1906), Tempkin (Tempkin & Pyzhev 1940), Dubinin-Radushkevich (D-R) (Dąbrowski 2001), Redlich-Peterson (Redlich & Peterson 1959), and Sips (Blanchard *et al.* 1984) equations, which are shown in Table 2.

Adsorption thermodynamic

Adsorption thermodynamics is the realization of the adsorption process, and is a means of identifying whether the adsorption process is feasible or not feasible. The changes in the adsorption free energy can be calculated using Equation (12):

$$\Delta G = -RT\mathrm{Ln}K_{eq} \tag{12}$$

where ΔG is the change in Gibbs free energy, and K_{eq} is the equilibrium constant.

The change in enthalpy and the entropy can be found by plotting the natural logarithm of the concentration of BR18 in the solution at equilibrium (C_{Se}, mg/L) divided by the concentration of BR18 on the adsorbent at equilibrium (C_{Ae}, mg/L) and the inverse of the temperature (T, K) as shown in Equation (13):

$$\ln\frac{C_{Se}}{C_{Ae}} = -\frac{\Delta H}{RT} + \frac{\Delta S}{R} \tag{13}$$

The change in enthalpy of biosorption (ΔH°) and the change in standard entropy (ΔS°) are a function of the change in free energy, as shown in Equation (14)

$$\Delta G^\circ = \Delta H^\circ - T\Delta S^\circ \tag{14}$$

Desorption studies

Desorption studies were done as described in a previous works (Saleh *et al.* 2019). Briefly, at the end of the adsorption process, the adsorbent was separated from the aqueous solution. First, the effect of acid type was investigated and HCl, H_2SO_4, HNO_3, and H_3PO_4 were tested. Second, different molarities of the acid (0.5, 1, 2.5, and 5 M) were tested. The desorption conditions were selected to be the same as the adsorption conditions (agitation speed: 150 rpm, solution volume: 50 mL, temperature: 25 ± 2 °C). The desorption efficiency was calculated using Equation (15):

$$\text{Desorption efficiency } \% = \frac{\text{Desorbed dye concentration}}{\text{Adsorbed dye concentration}} \times 100 \tag{15}$$

Table 3 | The physical properties for the adsorbent at different particle sizes

Parameter	Unit	< 45 μm	45–106 μm	> 106 μm
BET surface area	(m^2/g)	25.27180	11.03790	5.22000
Total pore volume	(cm^3/g)	0.11298	0.04515	0.01018
Micropore volume	(cm^3/g)	0.06897	0.00635	0.02487
Mesoporous volume	(cm^3/g)	0.00109	0.00022	0.00059
Pore diameter	nm	17.88191	16.36362	7.79847

Table 4 | The elemental composition of the adsorbent before and after adsorption

	Before adsorption		After adsorption	
Element	Weight (%)	Atomic (%)	Weight (%)	Atomic (%)
C	62.58	68.31	60.88	66.91
N	9.55	8.91	11.06	10.42
O	27.64	22.65	26.91	22.20
Na	0.07	0.04	0.30	0.17
Cl	0.05	0.02	0.42	0.16
Ca	0.11	0.04	0.43	0.14

RESULTS AND DISCUSSION

Hydrochar characterization

The prepared hydrochar was sieved <45 μm, 45–106 μm, and >106 μm and analysed by BET analysis using the adsorption and desorption of N_2 gas. Three different particle sizes were analysed to determine the physical properties of the adsorbent. BET surfaces areas, the total, micropore and mesopore volumes of the pores, microporous volumes, and the pore diameters were measured; they are shown in Table 3.

As shown in Table 3, the adsorbent with a particle size of less than 45 μm has the maximum surface area, with a value of 25.2718 m^2/g. Also, the total pore volume is inversely related to particle size. The maximum pore diameter is 17.88 nm, which is larger than the BR18 molecule. This reflects that the dye can be adsorbed by the pores of the adsorbent.

The hydrochar surface morphology was also identified by SEM analysis before and after adsorption to note the changes, which are shown in Figure 2. As shown in Figures 2(a) and 2(b), the adsorbent has a heterogeneous, rough, and porous surface. The SEM results also confirm the adsorption of BR18 onto the surface of the prepared hydrochar since the pores were filled and no pores were visible after the absorption process (Figures 2(c) and 2(d)).

Energy dispersive X-ray analysis (EDX) was carried out to determine the elements in the adsorbents. A comparison between the raw adsorbent and the adsorbent at the end of the adsorption process is shown in Table 4. Carbon, nitrogen, and oxygen are the dominant elements in the adsorbent. The concentrations of nitrogen and chlorine increased by the end of the adsorption process. This is further proof that the adsorption of BR18 onto the *Q. coccifera* acorn hydrochar had occurred successfully, as BR18 has nitrogen and chlorine elements in its structure.

FTIR analysis for the adsorbent on its own and with the dye was performed and the results are shown in Figure 3.

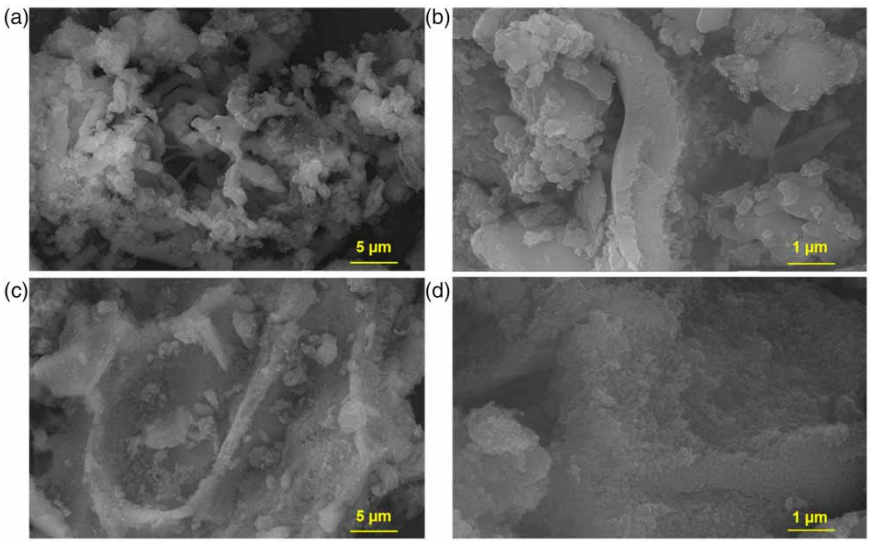

Figure 2 | SEM of the prepared adsorbent before the adsorption process for (a) 5 μm, (b) 1 μm and after the adsorption process for (c) 5 μm, (d) 1 μm.

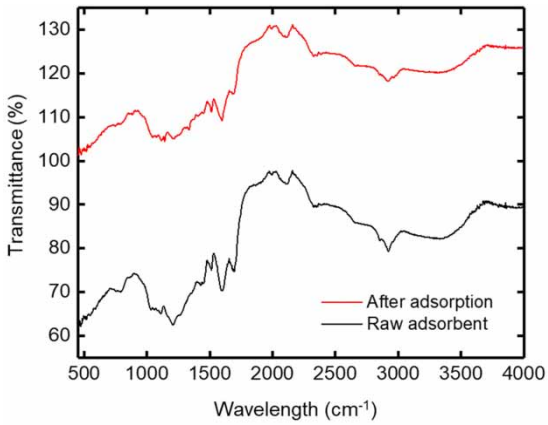

Figure 3 | FTIR analysis for the adsorbent before and after the adsorption process.

There are some changes between the FTIR for the adsorbent before and after it. The alkene compound class (functional group C = C bending) observed at peak 790 cm^{-1} before adsorption disappeared after it. Also, the peak at the band 1,428 cm^{-1} with functional group O-H bending was not visible at the end of the adsorption process. In contrast, three peaks were recorded for the band from 1,141 to 1,336 cm^{-1}. The peak at the band 1,141.65 cm^{-1} can be related to an amine compound with a functional group of C-N stretching. The functional group C-O stretching was also visible at the band of 1,213.01 cm^{-1}. The peak 1,336 cm^{-1} was related to the O-H bending functional group. In addition to these changes, peak shifting was visible at many bands. The FTIR results support the adsorption process.

The effect of pH

The concentration of hydrogen ions (pH) is the most important parameter in the adsorption process. It controls the protonation and deprotonation process on the adsorbent surface. To explore the effect of pH on the removal efficiency of the BR18 by adsorption, 1 g/L of the adsorbent was added to 100 mg/L of the dye concentration at constant temperature (25 ± 2 °C) and agitated at a speed of 150 rpm. The effects of pH on the adsorption capacity and removal efficiency are shown in Figure 4(a). The dye uptake and the adsorption capacity increased with increasing pH. The removal efficiency increased from 2% at pH 2 to 72% at pH 10. The capacity increased from 2 mg/g to 80 mg/g.

The zeta potential analysis for the adsorbent and the adsorbate under different pH values was studied. The adsorbent and the adsorbate were dissolved in 25 mL of distilled water and measured using a zeta meter (Malvern Zeta Sizer Nano ZS). The zeta potentials for the adsorbent at all pH values were negative (Figure 4(b)), while for the adsorbate they were positive at all the measured pH values. Because the adsorbent and the adsorbate have different charges, they will be an attractive force between them. The values of the zeta potential for the adsorbent sharply decreased from −5.87 mV at pH 2 to −43.93 mV at pH 10. As the zeta potential for the adsorbent decreased with increasing pH, the attractive force between the hydrochar and BR18 increased, which resulted in the increasing removal efficiency.

The effect of particle size

The effect of the adsorbent's particle size on the adsorption efficiency was investigated. Three different particle sizes were used in the experiments while the other parameters were kept constant (dye concentration: 110 mg/L, contact time: 60 min, adsorbent dosage: 1 g/L, and volume: 50 mL). The results showed that the maximum removal efficiency was obtained when the particle size was smaller than

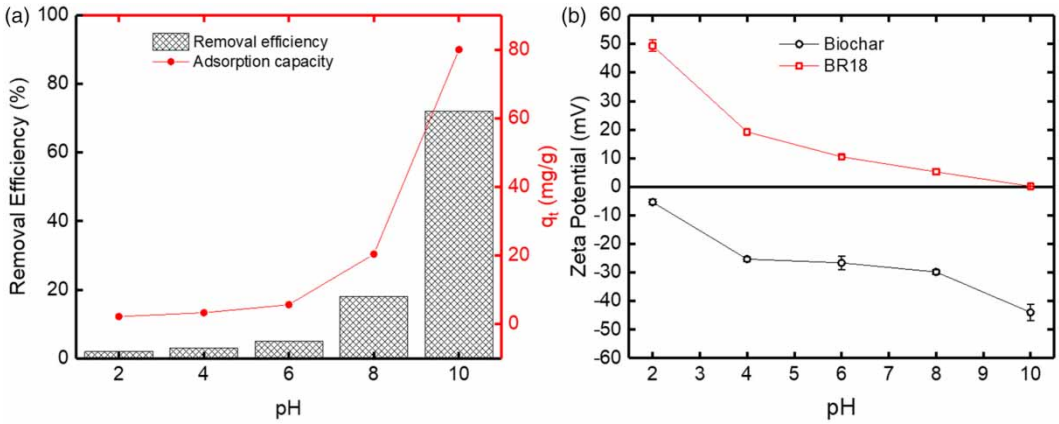

Figure 4 | (a) Effect of pH on the removal efficiency and adsorption capacity and (b) zeta potential values for the adsorbent and BR18.

Table 5 | Effect of particle size on the removal efficiency of BR18 by *Q. coccifera* acorn hydrochar

Particle size	Initial concentration (mg/L)	Final concentration (mg/L)	Removal efficiency (%)
<45 μm	110	12	89.1
45–106 μm	110	18	83.6
>106 μm	110	30	72.7

45 μm, with an efficiency of 89.1% (Table 5). These results can be explained by the surface area of the adsorbent. As shown in BET results, the particle sizes have an inverse relationship with the surface area.

The effect of adsorbent amount

The effect of the adsorbent amount on the removal efficency was investigated. Hydrochar was added in different quantities (0.5, 1.0, 1.5 g/L) into solutions with a concentration of 125 mg/L BR18. The results show that the maximum removal efficiency occurred at 1.5 g/L (Table 6).

The effect of contact time and initial concentration

The effect of contact time (0–120 min) on the uptake of BR18 by *Q. coccifera* acorn hydrochar at an initial concentration of 280 mg/L was studied and the results are shown in Figure 5(a). The removal efficiency increased sharply for the first 5 min, after which the removal efficiency reached a steady state at 60 min, with a maximum removal of 87.9%. After that, the removal efficiency did not change and hence 60 min was chosen as the optimum contact time. The removal of BR18 from the aqueous solution had occurred in two steps: the rapid step (first 5 min) when the active sites on the adsorbent surface were empty; as the number of active sites decreased (occupied by the dye), the removal speed decreased, which was the second step.

Table 6 | Effect of hydrochar amount on the removal efficiency of BR18

Hydrochar amount (g/L)	Removal efficiency (%)
0.5	66%
1.0	76%
1.5	91%

Initial concentration is one of the most important factors affecting the adsorption process. The adsorption capacity for the prepared hydrochar at different initial concentrations is shown in Figure 5(b). The capacity increased sharply with the increase in initial concentration of BR18 up to 280.8 mg/L. Then the graph became flatter. This can be related to the availability of active sites. The capacity increased from 20.9 mg/g at a concentration of 40 mg/L to 194.6 mg/g at a concentration of 454 mg/L.

Kinetics studies

The obtained data were fitted to Lagergren's pseudo-first-order and pseudo-second-order models to determine the adsorption kinetics. The linear form of Lagergren's pseudo-first-order and pseudo-second-order expressed in Equations (3) and (4) were fitted at different concentrations to obtain the maximum correlation coefficients. The chi-square errors (X^2) were tested using the SciDavis program to study the linearization errors. Table 7 shows the kinetics model parameters and also shows the X^2 results. Because of the high values of the correlation coefficients, the X^2 errors being very small, and the calculated capacities being very close to the experimental capacities, the adsorption of

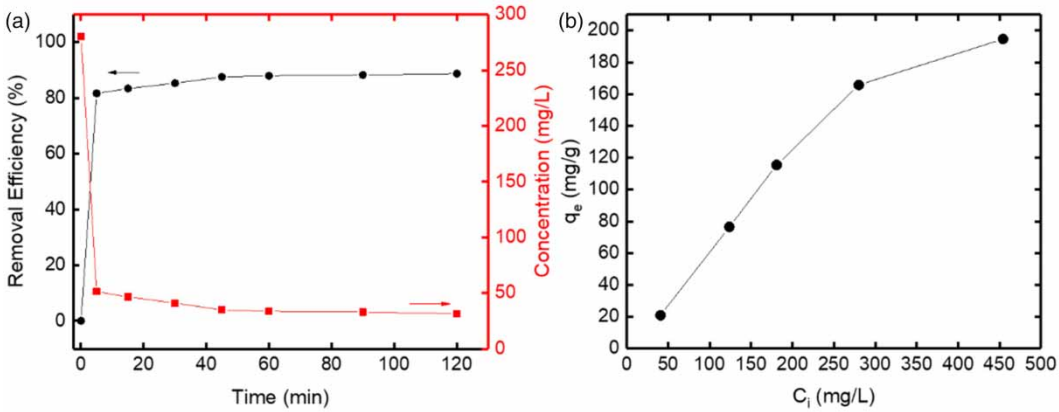

Figure 5 | (a) Change in removal efficiency and concentration over time and (b) change in adsorption capacity related to the initial concentration.

Table 7 | Lagergren's pseudo-first-order and pseudo-second-order parameters for the adsorption of BR18 onto *Q. coccifera* acorn hydrochar

	Pseudo-first-order					Pseudo-second-order				
Concentration (mg/L)	K_1	q_e measured (mg/g)	$q_{e\ fitted}$ (mg/g)	R^2	X^2	k_2	q_e measured (mg/g)	q_e fitted (mg/g)	R^2	X^2
40	0.0706	21.91	0.9315	0.8851	0.2403	2.29142×10^{-5}	21.91	20.96440	0.9999	2.21×10^{-5}
125	0.0887	76.45	1.1243	0.9185	0.259	2.72510×10^{-9}	76.45	75.60570	0.9998	0.0003
180	0.0757	115.43	1.1193	0.7543	0.6949	3.20783×10^{-8}	115.43	115.4659	0.9999	2.57×10^{-7}
280	0.0705	165.70	5.2322	0.7985	2.4232	2.02134×10^{-7}	165.7	166.7568	0.9999	1.82×10^{-5}
454	0.0382	197.33	5.1885	0.8551	0.2266	3.30412×10^{-7}	197.33	200.9411	0.9987	0.0003

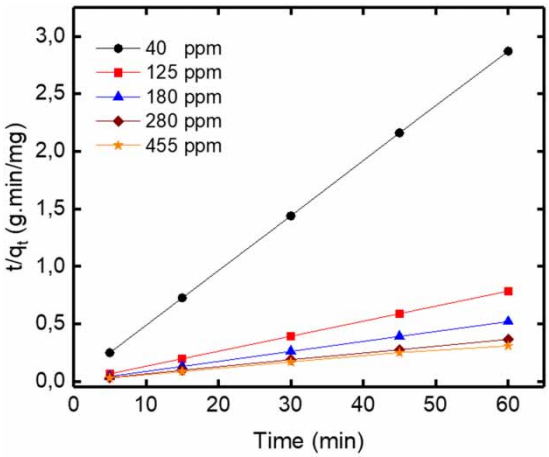

Figure 6 | Pseudo-second-order model for the adsorption of BR18 onto *Q. coccifera* acorn hydrochar at different concentrations.

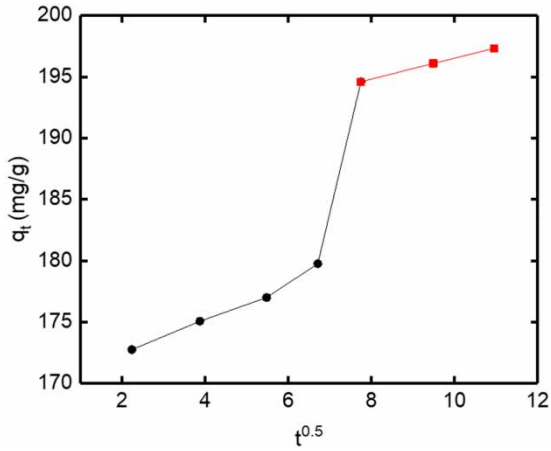

Figure 7 | Intraparticle diffusion model for the adsorption of BR18 onto *Q. coccifera* acorn hydrochar at different concentrations.

BR18 onto *Q. coccifera* acorn hydrochar is fitted to the pseudo-second-order model (Figure 6). According to this model, the rate of the adsorption is proportion to the available sites on the surface of the adsorbent.

According to Guo & Wang (2019), the pseudo-second-order model can occur in three ways: at low concentrations, at the final stage of adsorption, and when the adsorbent has abundant active sites (Qiu & Zheng 2009). The fitting of the current study to the pseudo-second-order model can be due to BR18 attaching to the active sites present on the surface of the prepared adsorbent. Unfortunately, neither Lagergren's pseudo-first-order nor pseudo-second-order models predict solute diffusion into the adsorbent.

The intraparticle diffusion model was used to determine the adsorption mechanism of BR18 onto *Q. coccifera* acorn hydrochar. The square root of time was plotted against the adsorption capacity, as shown in Figure 7. The intraparticle diffusion model plot shows multiple linear sections, but with none passing through the origin. The multilinearity reflects the effects of different mechanisms. The first mechanism indicates film diffusion, which involves BR18 moving slowly from the boundary layer to the surface of the *Q. coccifera* acorn hydrochar. The movement from the surface to the adsorbent pores and the attachment to the active pores reflects the second and third mechanisms. As a result of the intraparticle diffusion model graph, the main mechanism of the adsorption of BR18 onto *Q. coccifera* acorn hydrochar is film diffusion (graph has not passed through the origin), and intraparticle resistance has a role in the adsorption (because of multi-linearity).

Isotherms

The isotherms studies were carried out by exposing different dosages of the adsorbent to an initial BR18 concentration of 125 mg/L. The adsorbent and the adsorbate were agitated at 155 rpm and $25 \pm 2\ ^{\circ}C$. The samples were collected and fitted to the aforementioned isotherms. The isotherm parameters are shown in Table 8. In this study, the

Table 8 | Isotherm parameters for the adsorption of BR18 onto *Q. coccifera* acorn hydrochar

Isotherm	Parameter	Unit	Value
Langmuir	R^2	–	0.8988
	q_m	mg/g	263.1579
	b_{BR}	L/mg	0.0368
Freundlich	R^2	–	0.9527
	K_{BR}	(mg/g).(L/mg)	23.2113
	n	–	1.9550
Tempkin	R^2	–	0.9192
	b_T	–	42.7415
	A_T	L/g	0.0110
Dubinin-Radushkevich (D-R)	R^2	–	0.6980
	K_{ad}	mol^2/kJ^2	1e – 5
	q_s	mg/g	141.1750
Redlich-Peterson (R-P)	R^2	–	0.9483
	β	–	0.4885
	a_r	L/g	0.0431
Sips	R^2	–	0.8769
	r	–	0.9500
	q_m	mg/g	188.6793
	K_s	1/mg	0.0618

experimental data were fitted according to the four-parameter isotherms (Langmuir, Freundlich, Tempkin, Dubinin-Radushkevich (D-R)) and based on the three-parameter isotherms (Redlich-Peterson and Sips). The Langmuir isotherm has a correlation coefficient of 0.8988. The Langmuir assumes the adsorption process will reach the maximum capacity when a saturated monolayer is formed. The Freundlich isotherm has the highest correlation coefficient of 0.9527. This isotherm is an empirical isotherm, which assumes heterogeneous multilayer formation at the end of the adsorption process. The Tempkin isotherm ($R^2 = 0.9192$) includes the heat of the adsorption process. It assumes a linear inverse relationship between the heat of the molecule in the same layer and the surface coverage. The Dubinin-Radushkevich has the lowest coefficient, with an R^2 of 0.6980. The Redlich-Peterson ($R^2 = 0.9483$) depends on three parameters to describe the adsorption mechanism. It assumes the mechanism will be a mix of the Langmuir and Freundlich isotherms. According to R-P, no ideal monolayer will be formed. That Sips isotherm also has a relatively high correlation coefficient, with a value of 0.8769. The Sips isotherm can be defined as a combination of the Langmuir and Freundlich isotherms. At high concentrations, the Sips isotherm can be abbreviated to be the Langmuir isotherm. In contrast, it will be reduced to the Freundlich isotherm at low concentrations.

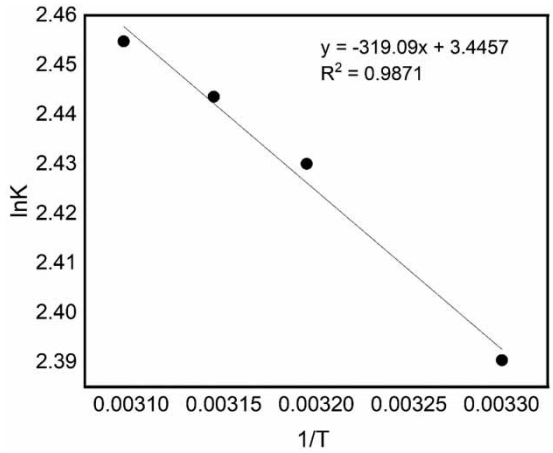

Figure 8 | The relation between temperature and the normal logarithm of K.

Thermodynamics

The thermodynamic parameters (Gibbs free energy, enthalpy, and entropy) were determined using Equations (12)–(14). The adsorption experiments were conducted at different temperatures (303, 313, 318, and 323 K). At the end of the adsorption experiments, the relationship shown in Equation (12) was plotted and is shown in Figure 8.

The change in enthalpy was found by multiplying the slope value by the universal gas constant. The multiplication of the universal gas constant with the graph intercept gave the entropy value. The Gibbs free energy for each temperature was determined using Equation (14). Table 9 shows the thermodynamic parameters. Based on the negative value of the Gibbs free energy, the adsorption process of BR18 onto the *Q. coccifera* acorn hydrochar can be considered to be feasible and spontaneous in nature. The adsorption process can be considered as physisorption since the Gibbs free energy is lower than 20 kJ/mol (Singh & Kaur 2013). The Gibbs free energy at 30 °C was −6.011 kJ/mol, which is higher than the Gibbs free energy for the removal of Methylene Blue onto bagasse hydrochar −1.24 kJ/mol (Biswas *et al.* 2020). The change in enthalpy was

Table 9 | The thermodynamic parameters for the adsorption of BR18 onto *Q. coccifera* acorn hydrochar

T (°C)	ΔH (kJ/mol)	ΔS (J/mol.K)	ΔG (kJ/mol)
30	2.670	28.648	−6.011
40			−6.297
45			−6.440
50			−6.584

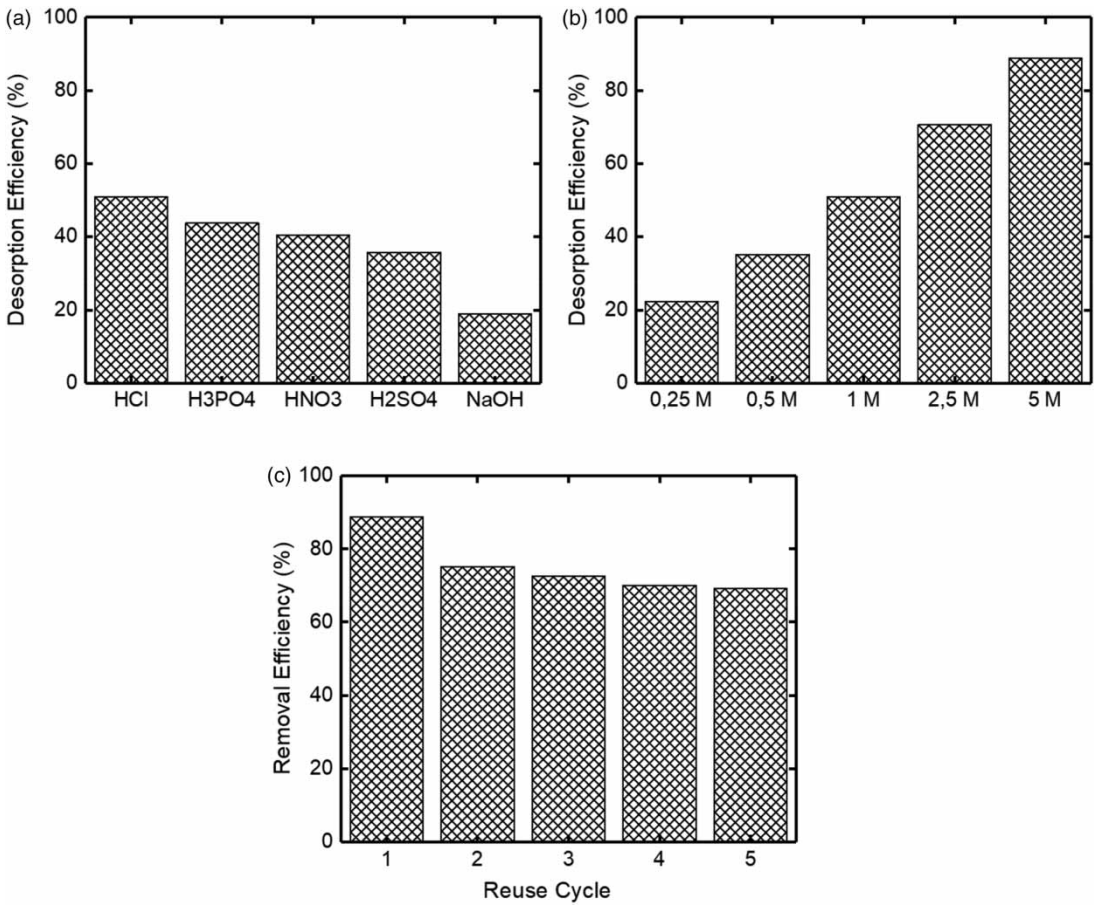

Figure 9 | Adsorption-desorption studies for BR18 dye. (a) The effect of acid and base type on BR18 dye desorption. (b) The effect of acid molarity on BR18 dye desorption. (c) Adsorption-desorption cycle.

found to be positive, so the adsorption process of BR18 onto *Q. coccifera* acorn hydrochar can be imagined as being endothermic. The positive entropy value reflects the solid phase randomness and the change in the surface of the adsorbent at the end of the adsorption process. Similar results were obtained by previous work (Afroze *et al.* 2016; Dawood *et al.* 2017; Biswas *et al.* 2020).

Desorption study

Desorption was investigated in the optimum conditions of the adsorption process. Different concentrations of HCl were tested. The desorption percentage increased with the concentration of HCl. The maximum desorption, 80.4%, was obtained at 5 M HCl. The adsorption-desorption process was repeated five times and the removal efficiencies after each cycle are shown in Figure 9. The removal efficiency of the BR18 from the aqueous solution by the prepared hydrochar in the first cycle was 90.4%. The desorption process was carried out several times, and after each cycle, the removal efficiency decreased until it leveled off in the fifth cycle. The removal efficiency in the fifth cycle was 69.2%.

The hydrochar prepared using SWM was used in the adsorption of azo dye. To investigate the feasibility of using this method to produce hydrochar, it was compared with other studies, as shown in Table 10.

CONCLUSION

In this study, the *Q. coccifera* acorn hydrochar was prepared successfully in SWM. This is an environmentally friendly method since no chemicals were used in the production of the hydrochar. Also, it can be considered to be an economical method as the preparation temperature did not exceed 240 °C, and the yield reached 72%.

Table 10 | Comparison with other studies

Raw material	Biochar/hydrochar preparation method	Adsorbate	Capacity (mg/g)	Isotherm	Kinetics	Thermodynamics	Reference
Palm petiole	Pyrolyzed at 700 °C	Crystal Violet	209.0	Langmuir	Empiric Avrami	Endothermic	Chahinez *et al.* (2020)
Bovine bones	Pyrolyzed at 800 °C	Basic Red 9	49.5	Langmuir	Pseudo-first-order	–	Côrtes *et al.* (2019)
Fish scales	Pyrolyzed at 800 °C	Basic Red 9	52.3	BET	Pseudo-first-order	–	Côrtes *et al.* (2019)
Municipal solid waste	Pyrolyzed at 400–800 °C	Methylene Blue	33.3	–	Pseudo-second-order	Endothermic	Chen *et al.* (2013)
Switchgrass	Pyrolyzed at 600 °C	Orange G	8.2	Langmuir	Pseudo-second-order	–	Park *et al.* (2019)
Cow dung	Pyrolyzed at 500 °C	Methylene Blue	19.2	Langmuir	Pseudo-second-order	Endothermic	Ahmad *et al.* (2020)
Sewage sludge	Pyrolyzed at 550 °C	Methylene Blue	29.8	Langmuir	Pseudo-second-order	Endothermic	De Filippis *et al.* (2013)
Q. coccifera acorns	SWM	Basic Red 18	194.6	Freundlich	Pseudo-second-order	Endothermic	This study

The prepared hydrochar was used as an adsorbent to remove BR18 from aqueous solution. The adsorption process of the BR18 onto the prepared hydrochar can be considered to be fast since a drop in concentration was noticed after 5 min. The adsorption process was significantly affected by pH concentration: the maximum removal efficiency was obtained at pH 10. The adsorption process was fitted to the Freundlich isotherm and pseudo-second-order model. The feasibility of the adsorption process was obtained from the thermodynamic experiments. The adsorption process was found to be spontaneous and endothermic in nature. The adsorbent was used for five cycles, and at the end of the fifth cycle, the efficiency was 70%. According to the these results, the hydrochar prepared by SWM can be used as an effective adsorbent for BR18 dye from and aqueous solution.

CONFLICT OF INTEREST

The authors have no conflict of interest in relation to this work.

DATA AVAILABILITY STATEMENT

All relevant data are included in the paper or its Supplementary Information.

REFERENCES

Abaide, E. R., Dotto, G. L., Tres, M. V., Zabot, G. L. & Mazutti, M. A. 2019 Adsorption of 2–nitrophenol using rice straw and rice husks hydrolyzed by subcritical water. *Bioresour. Technol.* **284**, 25–35. https://doi.org/10.1016/j.biortech.2019.03.110.

Afroze, S., Sen, T. K., Ang, M. & Nishioka, H. 2016 Adsorption of methylene blue dye from aqueous solution by novel biomass *Eucalyptus sheathiana* bark: equilibrium, kinetics, thermodynamics and mechanism. *Desalin. Water Treat.* **57**, 5858–5878. https://doi.org/10.1080/19443994.2015.1004115.

Ahmad, A., Khan, N., Giri, B. S., Chowdhary, P. & Chaturvedi, P. 2020 Removal of methylene blue dye using rice husk, cow dung and sludge biochar: characterization, application, and kinetic studies. *Bioresour. Technol.* **306**, 123202. https://doi.org/10.1016/j.biortech.2020.123202.

Al-Kdasi, A., Idris, A., Saed, K. & Guan, C. T. 2004 Treatment of textile wastewater by advanced oxidation processes – a review. *Glob. Nest J.* **6** (3), 223–230.

Antczak, A., Greta, M., Kopeć, A. & Otto, J. 2019 Characteristics of the textile industry of two Asian powers: China and India. Prospects for their further development on global markets. *Fibres Text. East. Eur.* **27**, 10–19. https://doi.org/10.5604/01.3001.0013.2895.

Asfaram, A., Ghaedi, M., Ghezelbash, G. R. & Pepe, F. 2017 Application of experimental design and derivative spectrophotometry methods in optimization and analysis of biosorption of binary mixtures of basic dyes from aqueous solutions. *Ecotoxicol. Environ. Saf.* **139**, 219–227. https://doi.org/10.1016/j.ecoenv.2017.01.043.

Banerjee, S., Dubey, S., Gautam, R. K., Chattopadhyaya, M. C. & Sharma, Y. C. 2019 Adsorption characteristics of alumina nanoparticles for the removal of hazardous dye, orange G from aqueous solutions. *Arab. J. Chem.* **12**, 5339–5354. https://doi.org/10.1016/j.arabjc.2016.12.016.

Barrett, E. P., Joyner, L. G. & Halenda, P. P. 1951 The determination of pore volume and area distributions in porous substances. I. Computations from nitrogen isotherms. *J. Am. Chem. Soc.* **73**, 373–380. https://doi.org/10.1021/ja01145a126.

Bayramoglu, G., Kunduzcu, G. & Arica, M. Y. 2020 Preparation and characterization of strong cation exchange terpolymer resin as effective adsorbent for removal of disperse dyes. *Polym. Eng. Sci.* **60**, 192–201. https://doi.org/10.1002/pen.25272.

Biswas, S., Mohapatra, S. S., Kumari, U., Meikap, B. C. & Sen, T. K. 2020 Batch and continuous closed circuit semi-fluidized bed operation: removal of MB dye using sugarcane bagasse biochar and alginate composite adsorbents. *J. Environ. Chem. Eng.* **8**, 103637. https://doi.org/10.1016/j.jece.2019.103637.

Blanchard, G., Maunaye, M. & Martin, G. 1984 Removal of heavy metals from waters by means of natural zeolites. *Water Res.* **18**, 1501–1507. https://doi.org/10.1016/0043-1354(84)90124-6.

Brião, G. V., Jahn, S. L., Foletto, E. L. & Dotto, G. L. 2018 Highly efficient and reusable mesoporous zeolite synthetized from a biopolymer for cationic dyes adsorption. *Coll. Surf. A Physicochem. Eng. Asp.* **556**, 43–50. https://doi.org/10.1016/j.colsurfa.2018.08.019.

Chahinez, H.-O., Abdelkader, O., Leila, Y. & Tran, H. N. 2020 One-stage preparation of palm petiole-derived biochar: characterization and application for adsorption of crystal violet dye in water. *Environ. Technol. Innov.* **19**, 100872. https://doi.org/10.1016/j.eti.2020.100872.

Chen, H., Zhang, C. H. & Wang, T. 2013 Adsorption of methylene blue onto char from pyrolysis of municipal solid waste. *Appl. Mech. Mater.* **345**, 163–166. https://doi.org/10.4028/www.scientific.net/AMM.345.163.

Chong, K. Y., Chia, C. H., Zakaria, S. & Sajab, M. S. 2014 Vaterite calcium carbonate for the adsorption of Congo red from aqueous solutions. *J. Environ. Chem. Eng.* **2**, 2156–2161.

Chuntanapum, A. & Matsumura, Y. 2009 Formation of tarry material from 5-HMF in subcritical and supercritical water. *Ind. Eng. Chem. Res.* **48**, 9837–9846. https://doi.org/10.1021/ie900423 g.

Côrtes, L. N., Druzian, S. P., Streit, A. F. M., Godinho, M., Perondi, D., Collazzo, G. C., Oliveira, M. L. S., Cadaval, T. R. S. & Dotto, G. L. 2019 Biochars from animal wastes as alternative materials to treat colored effluents containing basic red 9. *J. Environ. Chem. Eng.* **7**, 103446. https://doi.org/10.1016/j.jece.2019.103446.

Crini, G. & Lichtfouse, E. 2019 Advantages and disadvantages of techniques used for wastewater treatment. *Environ. Chem. Lett.* **17**, 145–155. https://doi.org/10.1007/s10311-018-0785-9.

Dąbrowski, A. 2001 Adsorption – from theory to practice. *Adv. Coll. Inter. Sci.* **93**, 135–224. https://doi.org/10.1016/S0001-8686(00)00082-8.

Darwesh, O. M., Matter, I. A. & Eida, M. F. 2019 Development of peroxidase enzyme immobilized magnetic nanoparticles for bioremediation of textile wastewater dye. *J. Environ. Chem. Eng.* **7**, 102805. https://doi.org/10.1016/j.jece.2018.11.049.

Dawood, S., Sen, T. K. & Phan, C. 2017 Synthesis and characterization of slow pyrolysis pine cone bio-char in the removal of organic and inorganic pollutants from aqueous solution by adsorption: kinetic, equilibrium, mechanism and thermodynamic. *Bioresour. Technol.* **246**, 76–81. https://doi.org/10.1016/j.biortech.2017.07.019.

De Filippis, P., Di Palma, L., Petrucci, E., Scarsella, M. & Verdone, N. 2013 Production and characterization of adsorbent materials from sewage sludge by pyrolysis. In: *Chemical Engineering Transactions*. https://doi.org/10.3303/CET1332035.

dos Santos, A. J., Garcia-Segura, S., Dosta, S., Cano, I. G., Martínez-Huitle, C. A. & Brillas, E. 2019 A ceramic electrode of ZrO2-y2o3 for the generation of oxidant species in anodic oxidation. Assessment of the treatment of Acid Blue 29 dye in sulfate and chloride media. *Sep. Purif. Technol.* **228**, 115747. https://doi.org/10.1016/j.seppur.2019.115747.

Dotto, J., Fagundes-Klen, M. R., Veit, M. T., Palácio, S. M. & Bergamasco, R. 2019 Performance of different coagulants in the coagulation/flocculation process of textile wastewater. *J. Clean. Prod.* **208**, 656–665. https://doi.org/10.1016/j.jclepro.2018.10.112.

Elumalai, S. & Saravanan, G. K. 2016 The role of microalgae in textile dye industrial waste water recycle (phycoremediation). *Int. J. Pharma Bio Sci.* **7** (4), 662–673. https://doi.org/10.22376/ijpbs.2016.7.4.b662-673

Fang, G., Gao, J., Liu, C., Dionysiou, D. D., Wang, Y. & Zhou, D. 2014 Key role of persistent free radicals in hydrogen peroxide activation by biochar: implications to organic contaminant degradation. *Environ. Sci. Technol.* **48**, 1902–1910. https://doi.org/10.1021/es4048126.

Fathy, N. A., El-Shafey, S. & El-Shafey, O. I. 2017 Synthesis of a novel MnO2@carbon nanotubes-graphene hybrid catalyst (MnO2@CNT-G) for catalytic oxidation of basic red 18 dye (BR18). *J. Water Process Eng.* **17**, 95–101.

Freundlich, H. M. F. 1906 Adsorption in solution. *Z. Phys. Chem.* **57**, 385–471.

Guo, X. & Wang, J. L. 2019 A general kinetic model for adsorption: theoretical analysis and modeling. *J. Mol. Liq.* **288**, 111100. https://doi.org/10.1016/j.molliq.2019.111100.

Gupta, V. K. & Suhas. 2009 Application of low-cost adsorbents for dye removal – A review. *J. Environ. Manage.* **90**, 2313–2342. https://doi.org/10.1016/j.jenvman.2008.11.017.

Gupta, V. K., Bhushan, R., Nayak, A., Singh, P. & Bhushan, B. 2014 Biosorption and reuse potential of a blue green alga for the removal of hazardous reactive dyes from aqueous solutions. *Bioremediat. J.* **18**, 179–191. https://doi.org/10.1080/10889868.2014.918574.

Jegatheesan, V., Pramanik, B. K., Chen, J., Navaratna, D., Chang, C.-Y. & Shu, L. 2016 Treatment of textile wastewater with membrane bioreactor: a critical review. *Bioresour. Technol.* **204**, 202–212. https://doi.org/10.1016/j.biortech.2016.01.006.

Krastanov, A., Koleva, R., Alexieva, Z. & Stoilova, I. 2013 Decolorization of industrial dyes by immobilized mycelia of

Trametes versicolor. *Biotechnol. Biotechnol. Equip.* **27**, 4263–4268. https://doi.org/10.5504/BBEQ.2013.0096.

Kumar, S. & Gupta, R. B. 2009 Biocrude production from switchgrass using subcritical water. *Energy Fuels* **23**, 5151–5159. https://doi.org/10.1021/ef900379p.

Langmuir, I. 1918 The adsorption of gases on plane surfaces of glass, mica and platinum. *J. Am. Chem. Soc.* **40**, 1361–1403. https://doi.org/10.1021/ja02242a004.

Lavanya, C., Dhankar, R., Chhikara, S. & Sheoran, S. 2014 Review article degradation of toxic dyes: a review. *Int. J. Curr. Microbiol. Appl. Sci.* **3** (6), 189–199.

Lee, J., Sarmah, A. K. & Kwon, E. E. 2019 Production and Formation of Biochar. In: *Biochar From Biomass and Waste*. Elsevier, pp. 3–18. https://doi.org/10.1016/B978-0-12-811729-3.00001-7.

Li, Y. & Wang, Y. 2019 Double decoupling effectiveness of water consumption and wastewater discharge in China's textile industry based on water footprint theory. *PeerJ* **7**, e6937. https://doi.org/10.7717/peerj.6937.

Martorell, M. M., Rosales Soro, M. d. M., Pajot, H. F. & de Figueroa, L. I. C. 2018 Optimization and mechanisms for biodecoloration of a mixture of dyes by *Trichosporon akiyoshidainum* HP 2023. *Environ. Technol.* **39**, 3169–3180. https://doi.org/10.1080/09593330.2017.1375024.

Miklos, D. B., Remy, C., Jekel, M., Linden, K. G., Drewes, J. E. & Hübner, U. 2018 Evaluation of advanced oxidation processes for water and wastewater treatment – A critical review. *Water Res.* **139**, 118–131. https://doi.org/10.1016/j.watres.2018.03.042.

Nagpal, N. & Kakkar, R. 2020 Selective adsorption and separation of toxic cationic dyes using hierarchically porous SDBS modified vaterite microspheres (Hr-SMV). *J. Phys. Chem. Solids* **146**, 109598.

Naje, A. S., Chelliapan, S., Zakaria, Z., Ajeel, M. A. & Alaba, P. A. 2016 A review of electrocoagulation technology for the treatment of textile wastewater. *Rev. Chem. Eng.* **33** (3). https://doi.org/10.1515/revce-2016-0019.

Nural, Y., Gemili, M., Yabalak, E., De, C. L. M. & Ulger, M. 2018 Green synthesis of highly functionalized octahydropyrrolo[3,4-c]pyrrole derivatives using subcritical water, and their anti(myco)bacterial and antifungal activity. *Arkivoc* **2018**, 51–64. https://doi.org/10.24820/ark.5550190.p010.573.

Park, J.-H., Wang, J. J., Meng, Y., Wei, Z., DeLaune, R. D. & Seo, D.-C. 2019 Adsorption/desorption behavior of cationic and anionic dyes by biochars prepared at normal and high pyrolysis temperatures. *Colloids Surfaces A Physicochem. Eng. Asp.* **572**, 274–282. https://doi.org/10.1016/j.colsurfa.2019.04.029.

Patel, H. & Vashi, R. T. 2015 Batch Adsorption Treatment of Textile Wastewater. In: *Characterization and Treatment of Textile Wastewater*. Elsevier, pp. 111–125. https://doi.org/10.1016/B978-0-12-802326-6.00004-6.

Pearce, C. I., Christie, R., Boothman, C., von Canstein, H., Guthrie, J. T. & Lloyd, J. R. 2006 Reactive azo dye reduction by *Shewanella* strain J18 143. *Biotechnol. Bioeng.* **95**, 692–703. https://doi.org/10.1002/bit.21021.

Qiu, W. & Zheng, Y. 2009 Removal of lead, copper, nickel, cobalt, and zinc from water by a cancrinite-type zeolite synthesized from fly ash. *Chem. Eng. J.* **145**, 483–488. https://doi.org/10.1016/j.cej.2008.05.001.

Rafatullah, M., Sulaiman, O., Hashim, R. & Ahmad, A. 2010 Adsorption of methylene blue on low-cost adsorbents: a review. *J. Hazard. Mater.* **177**, 70–80. https://doi.org/10.1016/j.jhazmat.2009.12.047.

Redlich, O. & Peterson, D. L. 1959 A useful adsorption isotherm. *J. Phys. Chem.* **63**, 1024–1024. https://doi.org/10.1021/j150576a611.

Rosales, E., Pazos, M., Longo, M. A. & Sanromán, M. A. 2009 Electro-Fenton decoloration of dyes in a continuous reactor: a promising technology in colored wastewater treatment. *Chem. Eng. J.* **155**, 62–67. https://doi.org/10.1016/j.cej.2009.06.028.

Saleh, M., Yalvaç, M. & Arslan, H. 2019 Optimization of remazol brilliant blue R adsorption onto *Xanthium italicum* using the response surface method. *Karbala Int. J. Mod. Sci.* **5**. https://doi.org/10.33640/2405-609X.1017.

Schneider, P. 1995 Adsorption isotherms of microporous-mesoporous solids revisited. *Appl. Catal. A Gen.* **129**, 157–165. https://doi.org/10.1016/0926-860X(95)00110-7.

Singh, J. & Kaur, G. 2013 Freundlich, Langmuir adsorption isotherms and kinetics for the removal of malachite green from aqueous solutions using agricultural waste rice straw. *Int. J. Environ. Sci.* **4** (3). https://doi.org/10.6088/ijes.2013040300004.

Tan, I. A. W., Ahmad, A. L. & Hameed, B. H. 2008 Adsorption of basic dye on high-surface-area activated carbon prepared from coconut husk: equilibrium, kinetic and thermodynamic studies. *J. Hazard. Mater.* **154**, 337–346. https://doi.org/10.1016/j.jhazmat.2007.10.031.

Tempkin, M. J. & Pyzhev, V. 1940 Recent modification to Langmuir isotherms. *Acta Physiochem. USSR*. https://doi.org/10.1016/0016-3287(93)90022-L.

Verma, A. K., Dash, R. R. & Bhunia, P. 2012 A review on chemical coagulation/flocculation technologies for removal of colour from textile wastewaters. *J. Environ. Manage.* **93**, 154–168. https://doi.org/10.1016/j.jenvman.2011.09.012.

Yabalak, E. 2018a An approach to apply eco-friendly subcritical water oxidation method in the mineralization of the antibiotic ampicillin. *J. Environ. Chem. Eng.* **6**, 7132–7137. https://doi.org/10.1016/j.jece.2018.10.010.

Yabalak, E. 2018b Degradation of ticarcillin by subcritical water oxidation method: application of response surface methodology and artificial neural network modeling. *J. Environ. Sci. Heal. Part A* **53**, 975–985. https://doi.org/10.1080/10934529.2018.1471023.

First received 3 November 2020; accepted in revised form 15 December 2020. Available online 29 December 2020